Post-print of: Jasik P., Kozicki J., Kilich T., Sienkiewicz J., Henriksen N.: Electronic structure and rovibrational predissociation of the 2^1Π state in KLi. PHYSICAL CHEMISTRY CHEMICAL PHYSICS. Vol. 20, iss. 27 (2018), p. 18663-18670. DOI: 10.1039/c8cp02551g

Electronic structure and rovibrational predissociation of the $2^1\Pi$ state in KLi

P. Jasik[a], J. Kozicki [b], T. Kilich[a], J. E. Sienkiewicz [a*] and N. E. Henriksen[c]

Adiabatic potential energy curves of the $3^1\Sigma^+$, $3^3\Sigma^+$, $2^1\Pi$ and $2^3\Pi$ states correlating for large internuclear distance with the K(4s) + Li(2p) atomic asymptote were calculated. Very good agreement between the calculated and the experimental curve of the $2^1\Pi$ state allowed for a reliable description of the dissociation process through a small (~ 20 cm^{-1} for $J = 0$) potential energy barrier. The barrier supports several rovibrational quasi-bound states and explicit time evolution of these states via the time-dependent nuclear Schrödinger equation, showed that the state populations decay exponentially in time. We were able to precisely describe the time-dependent dissociation process of several rovibrational levels and found that our calculated spectrum match very well with the assigned experimental spectrum. Moreover, our approach is able to predict the positions of previously unassigned lines, particularly in the case of their low intensity.

1 INTRODUCTION

Studies of polar alkali dimers provide valuable insight into several basic phenomena, such as perturbations in excited states, potential curve crossings and avoided crossings, photodissociation, photoassociation, and new quantum matter, namely the Bose-Einstein condensate and ultracold two-fermionic species[1]. The development of spectroscopic methods allows for very accurate measurements, providing valuable data for the ground and excited states of these molecules. From the theoretical point of view heteronuclear alkali metal dimers are very attractive objects due to their simple electronic structure and the possibility of treating them as effective two-electron systems with separated atomic cores. Pseudopotential methods with longtail core polarization model potentials are well suited to treat such systems[2,3].

For years, the KLi dimer was an object of spectroscopic experiments[4–9] with the notable series of studies by the Warsaw group[10–15] which provided, using Doppler-free polarization labeling technique, molecular constants and potential energy curves for the ground and several excited singlet states up to $11^1\Pi$ lying 33,000 cm^{-1} above the minimum of the ground state. Some potential energy curves, like in the case of the $1^3\Sigma^+$ state[13], were determined experimentally despite limited data sets of vibrational energies. The KLi dimer was also studied in the field of ultracold atomic and molecular gases with strongly interacting two-fermionic species consisting of ^{40}K and ^{6}Li atoms[16–18].

Already in 1984, Müller and Meyer[19] performed extensive all-electron SCF calculations on KLi along with a careful treatment of intershell effects. In 1999, Rousseau et al.[20] performed CI calculations with nonempirical one-electron pseudopotentials and appropriate polarization potentials by means of the CIPSI program package[21] obtaining 58 electronic states of KLi. Recently extensive theoretical ab initio studies were performed, including the electronic structure, transition dipole moments[22], and effect of inner-shell electrons on the molecular properties[23]. Previously we have calculated the low-lying potential energy curves, transition dipole moments and Franck-Condon factors in order to show effective schemes of photoassociation reactions[24]. Also the electronic structure of KLi has been investigated by treating the K and Li atoms with the non-empirical relativistic effective core potentials[25]. Very recently, the multireference coupled cluster method (MRCC) has been used to calculate 10 low-lying states of KLi[26].

Important open questions concern the exact shape of potential energy curves (PEC) of excited states. The potential curve of the $2^1\Pi$ state derived from experiment[12,27] exhibits a rotationless barrier. The position of the maximum and height of the barrier are decisive in precise time-dependent calculations of levels which lie above the dissociation limit.

In our work, we address the problem of direct bound-to-free simulations, particularly for quasi-bound rovibrational levels lying just below the potential barrier. This is the energy region in which the good agreement between semi-classical and fully quantum results is questionable. We study the validity of the quantum bound-to-free approach near the potential barrier where quasi-bound levels are broad and their low intensity makes an additional challenge for experimentalists. We present the lines of par-

[a] Faculty of Applied Physics and Mathematics, Gdańsk University of Technology, Narutowicza 11/12, 80-233 Gdańsk, Poland
[b] Faculty of Civil and Environmental Engineering, Gdańsk University of Technology, Narutowicza 11/12, 80-233 Gdańsk, Poland
[*] E-mail: "J.E. Sienkiewicz" <jozef.sienkiewicz@pg.edu.pl>
[c] Department of Chemistry, Building 207, Technical University of Denmark, DK-2800 Kgs. Lyngby, Denmark.

tial cross section for predissociation along with time-dependent populations. Initial quasi-bound wavepackets with precisely assigned rotational and vibrational quantum numbers allows us to calculate the time-dependent population of rovibrational levels. To perform any time-dependent (dynamical) calculations it is preferable to have potential energy curves of high accuracy, this is essential in description of the predissociation process. Thus, the scope of our work includes calculations of potential energy curves with the special focus on the $2^1\Pi$ state and getting new insight into the dynamics of the rovibrational predissociation process. Details of this process showing the role of shapes of initial wavepackets in forming the spectral lines are shown step by step on the molecular movies (see Supplementary material[28]). To that end we show explicitly that the quasi-bound state populations decay exponentially in time. Moreover, our systematic study of energies and widths of quasi-bond levels provides new valuable data for finding affective photoassociation schemes leading to Bose-Einstein condensates. Whenever is possible we made careful comparison with available experimental data to get better insight into the nature of the predissociation process.

An overview of our computational method with the emphasis on the time-dependent method and boundary conditions is given in the next section. In Section 3, we discuss results for the $2^1\Pi$ state and compare them with the experimental data. Here also the spectrum and time-dependent population are presented and discussed. Conclusions are given in the last section.

2 THEORETICAL AND COMPUTATIONAL METHODS

2.1 Adiabatic potentials

For each alkali atom only the valence electron is treated explicitly. This approach with two valence electrons for the whole alkali molecule has been already described in our earlier papers and is proved to give reliable results, particularly for excited states[2,29–34]. Also, it can be applied for bigger molecules and even clusters, since the dimension of the active space and the number of configurations which has to be taken into account are relatively small.

Here the core electrons of K atoms are represented by the pseudopotential ECP18SDF[35]. We use the basis sets for potassium which come with ECP18SDF[36] for s and p functions and ECP10MDF pseudopotential[37] for d and f functions. Additionally, these basis sets are augmented by seventeen s functions, six p functions, ten d functions and six f functions. The exponential coefficients of the uncontracted Gaussian Type Orbitals (GTO) are listed in Supplementary material[28].

The core electrons of the Li atom are represented by the pseudopotential ECP2SDF[35]. The basis set for the s and p orbitals, which comes with this pseudopotential[36] is enlarged by functions for d and f orbitals given by Prascher *et al.*[38] and assigned by cc-pV5Z. Additionally, our basis set was augmented by six s short range correlation functions, seven p functions, seven d functions and five f functions. Also, we added to the basis the following set of diffuse functions: three s functions, four p functions, three d functions and three f functions. Coefficients of the exponents of the primitive Gaussian orbitals are listed in Supplementary material[28].

In our calculations of core polarization potentials, the static dipole polarizabilities of the atomic cores[35] are taken as 5.354 and 0.1915 a_0^3 for K and Li, respectively. In turn the cut-off parameters are equal to 0.296519 a_0^{-2} for K and 0.8351 a_0^{-2} for Li.

To calculate adiabatic potential energy curves of the KLi molecule we use the multiconfigurational self-consistent field/complete active space self-consistent field (MCSCF/CASSCF) method and the multi-reference singles and doubles configuration interaction (MRCISD) method. All calculations are performed by means of the MOLPRO program package[39]. We obtained adiabatic potential energy curves for four excited states, namely $^{1,3}\Sigma^+$ and $^{1,3}\Pi$ correlating to the K(4s)+Li(2p) atomic asymptote.

2.2 Molecular quantum dynamics

The time-dependent approach which is mathematically equivalent to the time-independent one can be regarded as a complementary tool and is often used in studying photodissociation processes. Here, it serves as an alternative and quite illustrative method for testing results of our structural calculations.

We start our consideration from the time-dependent Schrödinger equation written in the following form

$$\imath\hbar\frac{\partial}{\partial t}\Phi(R,t) = H_J^{nuc}\Phi(R,t), \tag{1}$$

where $\Phi(R,t)$ is the time-dependent wavepacket moving on the effective potential energy curve $U_J(R)$ and the nuclear Hamiltonian is taken as $H_J^{nuc} = -\frac{\hbar^2}{2\mu}\frac{\partial^2}{\partial R^2} + U_J(R)$.

The evolving wavepacket $\Phi(R,t)$ is a solution of Eq. (1). We choose as initial state, $\Phi(R,t=0) = \Psi_{E,J}(R)$, a quasi-bound state which can be calculated very accurately by the methods implemented in the program LEVEL[40]. This approach allows to calculate the population for the particular state labeled by (v,J). The wavepacket is tunneling away from its starting position with the main amplitude located inside the potential energy barrier. The time-dependent population $P(t)$ is calculated in the range from $R=0$ till R_{max}, where R_{max} is chosen sufficiently to the right of the outermost classical turning point such that $P(t=0)=1$. The population is calculated as

$$P(t) = \int_0^{R_{max}} |\Phi(R,t)|^2\, dR. \tag{2}$$

The process is also described by the time-dependent autocorrelation function

$$S(t) = \int \Phi^\star(R,t=0)\,\Phi(R,t)\, dR. \tag{3}$$

In our case the autocorrelation function describes the evolution of the initial nuclear eigenfunction in the excited electronic state.

We determine the spectrum by the inverse Fourier transform of $S(t)$[41] as follows

$$\sigma(E(v,J)) = \int_{-\infty}^{\infty} \mathrm{e}^{\imath E(v,J)t/\hbar} S(t)\, dt. \tag{4}$$

In our calculations the above integral is estimated over the range <0,T> with fast Fourier transform (FFT) routines[42].

A computer code for calculating the quantum dynamics[43–45] was implemented in a computational framework developed by one of the authors[46,47]. In our approach the Chebyshev polynomial recurrence relation formula[43,48] was modified by multiplying it by the absorbing boundary conditions term $e^{-\gamma(R)}$[49,50]. The resulting absorbing potential acts as the commonly used imaginary absorbing potential, such that the calculations are numerically stable in the Kosloff calculation method.

In the calculations of the autocorrelation function (Eq. 3), the propagation time is 1 ns which is sufficient for estimation of the integral in Eq. (4). In Eq. (2), we set the value of R_{max} to be equal to 57 a_0 (30 Å). There are 8192 points in the whole grid and 4669 points in the integration grid (since integration excludes the region of the absorbing boundary conditions). In order to avoid the interference between the outgoing and incoming waves on the periodic grid an absorbing potential is placed in the range from 57 to 100 a_0 (30 Å to 53 Å). This potential smoothly absorbs the wavepacket[49].

The obtained population curve $P(t)$ is roughly constant in the first 5 ps (see Fig. 1A), which is the time for the wavepacket to reach the R_{max} point. After this the population (Eq. 2) starts to decay. We observe that the population follows an exponential decay $e^{-t/\tau}$, with a decay constant τ. Here we demonstrate the exponential decay of population based on explicit time-propagation of a quasi-bound state. Often the exponential decay of such states is described by introducing an imaginary part in the state energies[41,51]. An exponential decay in population leads by using Eq. 4 to Lorentzian line shapes with FWHM equal to $\Gamma = \hbar/\tau$[41,51].

The time t_0 for best determination of the decay constant τ (and correspondingly Γ) was determined by performing a parametric least squares fitting, where the t_0 was adjusted in order to maximize the Pearson's correlation coefficient $r_{t_0,\Gamma}$ value of the fit (see Fig. 1B). The dependence of Γ on t_0 (at which the least squares fitting starts) is shown on Fig. 1C. It can be seen that a "perfect" fit of Γ is found in a very narrow range (see inset of Fig. 1C) in the order of 0.02 cm^{-1}. When scanning the entire time range $t_0 \in$[5 ps,1 ns], the least squares fitting had a tendency to produce "perfect" fits $r_{t_0,\Gamma} = 1.0$ at very large t_0 (of the order of 0.1 ns), hence to force inclusion of the beginning of the population decay (which starts around 5 ps) the fitting was constrained to start before $t_0 < 15$ ps.

3 RESULTS AND DISCUSSION

3.1 Born-Oppenheimer potentials

In order to obtain the broader picture besides the potential energy curve of the $2^1\Pi$ state, we present in Fig. 2 three other states correlating with the same atomic asymptote K(4s) + Li(2p). These are $3^1\Sigma^+$, $2^3\Pi$ and $3^1\Sigma^+$. A table with numerical values are available in Supplementary material[28]. The inset in Fig. 2 gives a closer view of the potential barriers, including the quite distinct one of the $2^1\Pi$ state, which plays an important role in the proper interpretation of a part of spectrum. Comparison between spectroscopic parameters calculated from our potential curves and those provided by experiment and other calculations are given in Tab. 1. The shape of our $3^1\Sigma^+$ potential curve is very close to the most recent experimental one[11], since the differences between respective parameters describing well depths D_e and harmonic frequencies ω_e are very small. Our calculated well minimum position R_e lies very close to the experimental ones[11,52], although the quite recent theoretical result of Daudouri et al.[22] lies even closer to the experimental values. There is no experimental data for the $3^3\Sigma^+$ state which has an exotic shape. Its well minimum lies on the energy scale above the dissociation limit and the well is adequately deep to support some quasi-bound levels with predicted ω_e around 152 cm^{-1}.

In case of the $2^1\Pi$ state, the comparison of our spectroscopic parameters R_e, D_e, ω_e and B_e gives a very good consistent agreement with experimental data of Grochola et al.[11]. It means that the description of the shape is very reliable. We also notice that two parameters R_e and D_e of the newest calculations of Musiał et al.[53] are even closer to experimental ones. For this state the precise theoretical description of the rotationless potential barrier is very important due to the existence of refined experimental data by Jastrzębski et al.[27]. The position of the barrier's maximum and its height for two available sets of experimental data and three chosen theoretical results are given in Tab. 2. In turn, Fig. 3 shows the comparison between experimental data and three theoretical results of the barrier shape. Appropriate differences (Fig. 3B) clearly show the almost perfect match between our potential barrier and the experimental one. The difference curve of Musiał et al.[53] shows systematic discrepancy of 15 cm^{-1} while the curve of Rousseau et al.[20] along with increase of internuclear distance shows substantial improvement and reasonable stabilization after crossing with the reference 0-line. The differences between experimental[27] and our theoretical term values of the levels supported by the potential barrier (Fig. 4) are rather small, not exceeding 4 cm^{-1} in the $v = 14$ level with the mean absolute error (MAE) equal to 2.78 cm^{-1} and only 0.5 cm^{-1} in the $v = 17$ level with MAE=0.38 cm^{-1}. In the case of $v = 15$ and 16 MAE equals to 1.62 and 0.71, respectively. The levels $v = 15$ and 16 exhibit strong perturbation with the visible shifts caused by interaction with the nearby $3^1\Sigma^+$ and $2^3\Pi$ states.

For the other triplet Π state there is no experimental data (Tab. 1). The comparison among theoretical results shows consistency between our R_e, D_e and ω_e parameters and those of Musiał et al.

3.2 Photodissociation dynamics

Using the computer code solving the time-dependent Schrödinger equation[43–47], we are able to calculate several interesting features of the spectra and where it is possible to compare them with the other theoretical results and experimental data. In Fig. 5 we compare our results of the level widths Γ (e.g. the full width at half maximum, FWHM) with those calculated from the program LEVEL[40]. Our line widths are calculated directly from the exponential decay of population. The extracted decay constant is used to estimate the width $\Gamma = \hbar/\tau$. The program LEVEL calculates the line width from a uniform semi-classical treatment.

Table 1 Spectroscopic parameters R_e [Å], D_e, ω_e, B_e, and T_e [cm^{-1}] for the excited states correlated in the atomic limit to the Li(2p) + K(4s) asymptote.

State	Author	R_e	D_e	ω_e	B_e	T_e
$3^1\Sigma^+$	present (theory)	4.158	3629	114.91	0.1628	17639
	Grochola 2002 (exp.) [11]	4.192	3619	115.41	0.1614	17501
	Pashov 1998 (exp.) [52]	4.190	3619	115.41	0.1615	17501
	Musiał 2017 (theory) [53]	4.169	3597	116.32		17452
	Musiał 2016 (theory) [26]	4.152	3369	110.92		17669
	Al-dossary 2014 (theory) [25]	4.154	3345			17699
	Dardouri 2012 (theory) [22]	4.186	3554	115.20		17767
	Rousseau 1999 (theory) [20]	4.128	3477	114.27	0.1649	17647
$3^3\Sigma^+$	present (theory)	3.762	-700	152.13	0.1980	22587
	Musiał 2017 (theory) [53]	3.783	-774	152.92		21823
	Musiał 2016 (theory) [26]	3.770	-876	163.93		21914
	Al-dossary 2014 (theory) [25]	3.837	-836			23865
	Dardouri 2012 (theory) [22]	3.773	-918			22616
$2^1\Pi$	present (theory)	4.028	1679	128.75	0.1737	19589
	Grochola 2003 (exp.) [12]	4.043	1664	128.98	0.1735	19456
	Musiał 2017 (theory) [53]	4.033	1664	132.62		19385
	Musiał 2016 (theory) [26]	4.000	1682	134.11		19356
	Al-dossary 2014 (theory) [25]	3.990	1438			20155
	Dardouri 2012 (theory) [22]	4.069	1300	120.92		20410
	Rousseau 1999 (theory) [20]	4.022	1584	132.30	0.1765	19541
$2^3\Pi$	present (theory)	4.030	811	103.65	0.1701	20457
	Musiał 2017 (theory) [53]	4.078	803	103.88		20246
	Musiał 2016 (theory) [26]	4.109	674	96.49		20365
	Al-dossary 2014 (theory) [25]	4.032	688			20458
	Dardouri 2012 (theory) [22]	4.011	612	123.60		21090
	Rousseau 1999 (theory) [20]	4.022	736	108.90	0.1732	20388

Table 2 Comparison of the barrier position R_{bar} [Å] and barrier height ΔE_{bar} [cm^{-1}] relative to the dissociation limit of the $2^1\Pi$ state with other theoretical and experimental results.

	This work	Exp. [27]	Exp. [12]	Theory (MRCC) [53]	Theory (pseudopotentials+CI) [20]
R_{bar}	7.98	8.20	7.79	7.93	7.62
ΔE_{bar}	20.73	20.80	26.50	20.35	27.50

It is observed that the semi-classical treatment overestimates the line widths for the broadest levels. Thus, the differences between the results become significant when the energy of quasi-bound levels approaches the top of the barrier. It is known that in this energy regime, the semi-classical approach does give less reliable results [40].

Our distribution of bound and quasi-bound levels for high vibrational numbers v exhibits several similarities to the experimental data (Fig. 6). For v =13, 14 and 15 the values of J which constitutes a boundary between bound and quasi-bound levels differs only by one. For v =16, because of strong perturbation with other states the comparison is impossible, while for $v = 17$, there is a perfect agreement. At last for v=18, no experimental data is available. The long broken vertical line placed at $J = 8$ crosses bound level with $v = 16$ and quasi-bound level with $v = 17$, and clearly illustrating that the last line with $v = 18$ in Fig. 7 comes from the virtual state lying above the potential barrier.

The part of our discrete spectrum calculated from Eq. 4 for the absorption transitions from the ground state level $v" = 3$, $J" = 8$ to the levels $v' = 16 - 18$, $J' = 8$ of $2^1\Pi$ is compared with the experimental spectrum in Fig. 7. According to our knowledge the remaining peaks in the spectrum are as yet not assigned by experimentalists. It should be noted that we have used the Condon approximation, i.e. a constant transition-dipole moment and the relative intensities of the peaks may change when this approximation is abandoned. The calculated spectrum is shifted by 744.835 cm^{-1} with respect to the data in Tab. 3. This shift was calculated in the following manner: the experimental energy 726.485 cm^{-1} [54] of the level $v" = 3$, $J" = 0$ in the ground state was incremented by 18.350 cm^{-1} which is the energy difference between the ground state levels $v" = 3$, $J" = 8$ and $v" = 3$, $J" = 0$. The agreement between our and experimental spectra is very satisfactory showing the usability of our methods in assigning particular transitions to quasi-bound levels. The process of quantum tunneling and forming the spectral lines can be viewed in the molecular movies (see Supplementary material [28]).

An overview of the calculated term energies may be found in Fig. 8. The present results of term values from $v = 8$ up to $v = 18$ show a characteristic pattern. The numerical values of level energies and widths of the $2^1\Pi$ state may be found in Tab. 3. Here

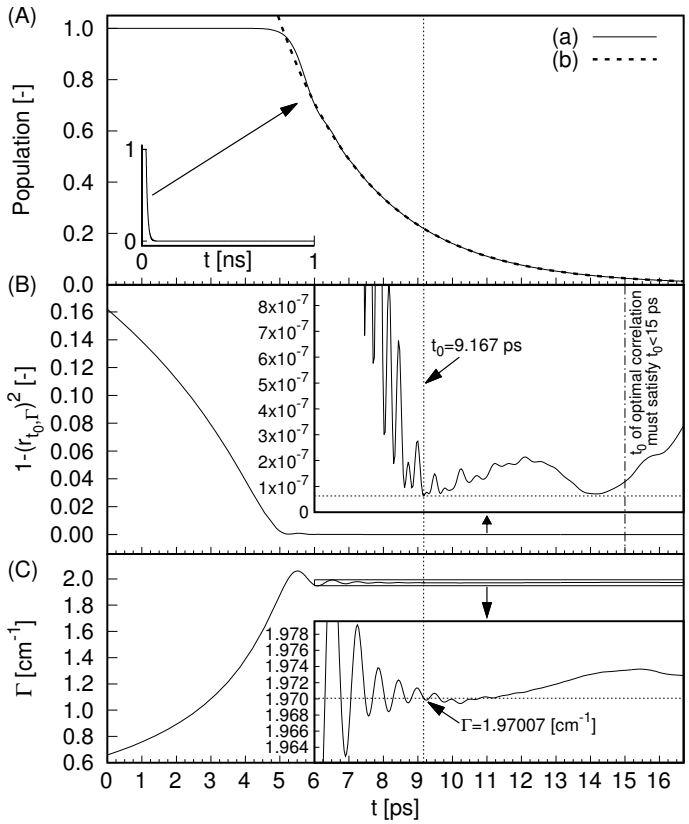

Fig. 1 The procedure of finding optimal FWHM Γ [cm^{-1}] shown for the level $J = 37$ and $v = 16$ of the $2^1\Pi$ state. (Aa) Population of time–evolving wavepacket is calculated up to 1 ns, but only the first 17 ps are shown here for clarity. (Ab) The obtained best fit population decay function $e^{-t/\tau}$, the population values to the left of t_0 were not used in the fit. (B) The value of Pearson's correlation coefficient $r_{t_0,\Gamma}$ (plotted as $1-(r_{t_0,\Gamma})^2$) as a function of time t_0 where the least squares fitting starts. (C) The value of FWHM Γ [cm^{-1}] obtained from least squares fitting starting at each t_0.

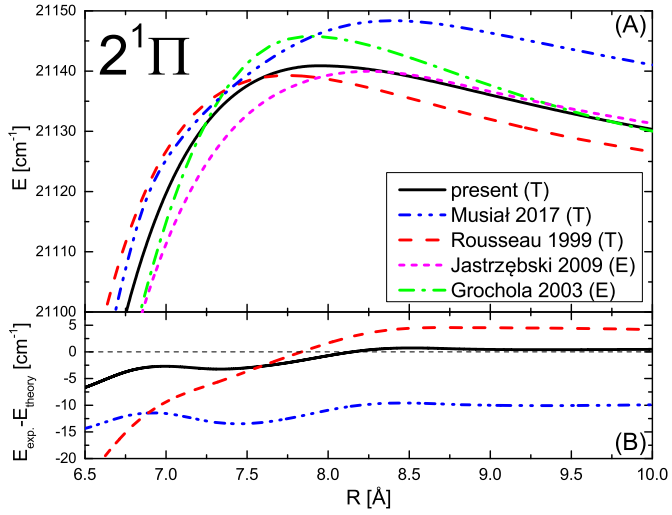

Fig. 3 (A) The potential energy barrier in the $2^1\Pi$ state. Present theoretical results (black solid line) are compared with results derived from experimental data by Jastrzębski et al.[27] (magenta short-dash line) and Grochola et al.[12] (green dash-dot line) as well as with the other recent theoretical results given by Musiał et al.[53] (blue dash-dot-dot line) and Rousseau et al.[20] (red-dash line). (B) Differences in energy between the experimentally determined potential[27] of the $2^1\Pi$ state and the present PEC as well as the other theoretical ones[20,53].

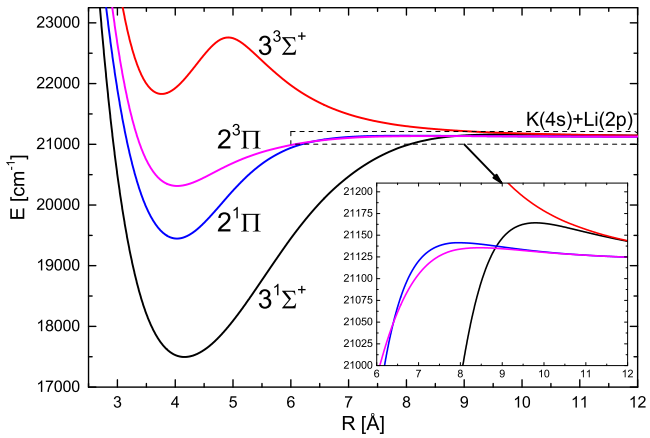

Fig. 2 Adiabatic potential energy curves of KLi correlating with the K(4s) + Li(2p) atomic asymptote.

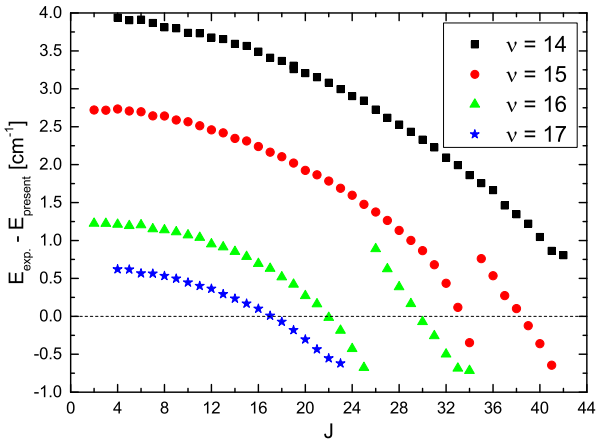

Fig. 4 Differences between experimental[27] and our calculated term values in the $v = 14$, 15, 16 and 17 levels of the $2^1\Pi$ state.

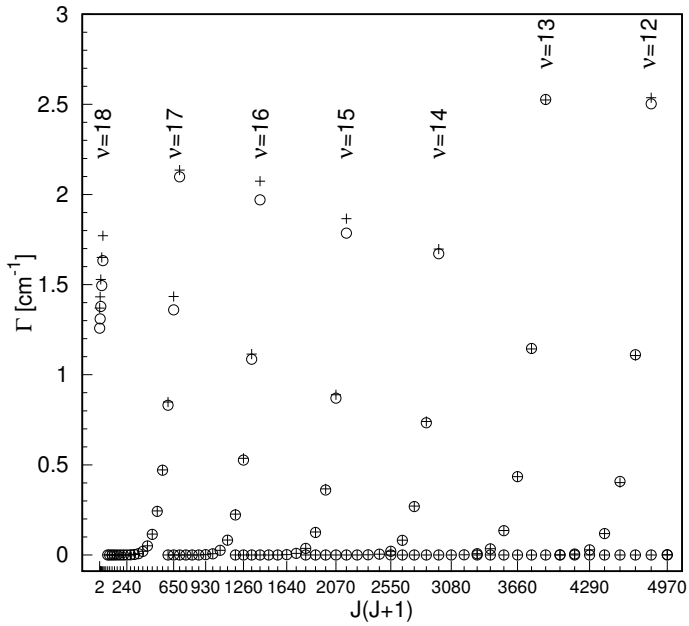

Fig. 5 Comparison of the widths of the bound ($\Gamma = 0$) and quasi-bound levels. Our results from bound-continuum time-dependent simulations are given by the open circles, while results obtained from the program LEVEL are given by crosses [40].

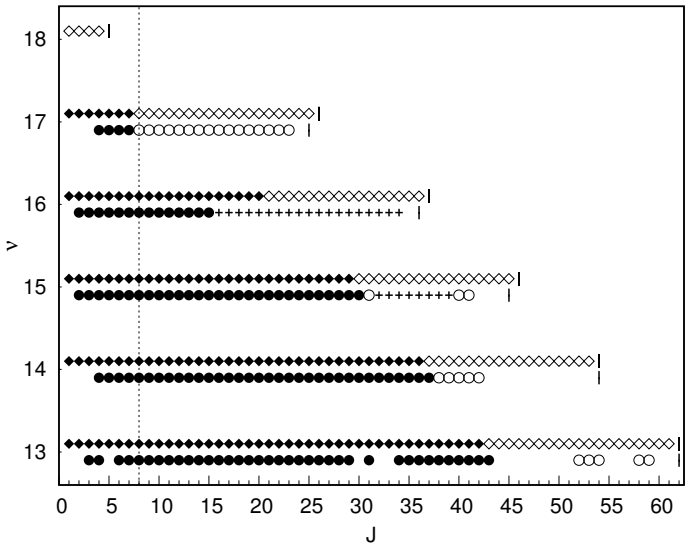

Fig. 6 Distribution of the present theoretical results (diamonds in the upper rows) and experimental data [27] (circles in the lower rows) for the high rovibrational levels in the $2^1\Pi$ state of KLi. Solid figures represent bound levels, open figures - quasi-bound levels, crosses - perturbed levels. Short vertical bars denote the last rotational level for each v. The long broken vertical line placed at $J = 8$ cuts v levels involved in transitions showed in Fig. 7 .

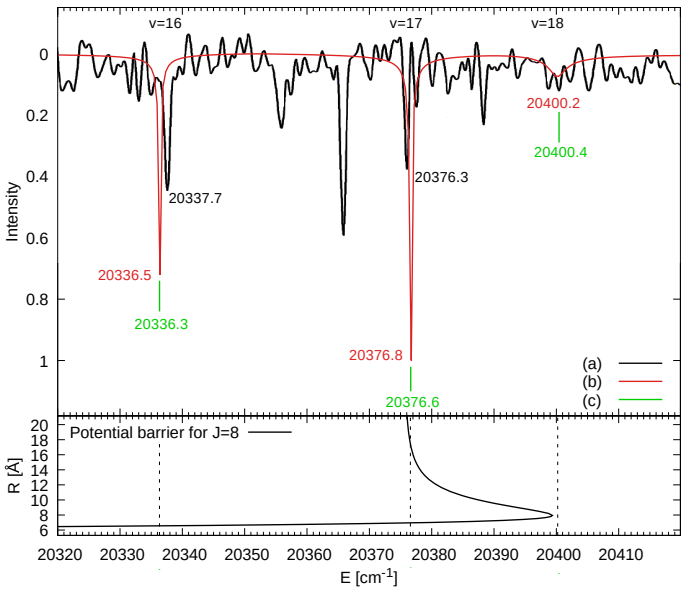

Fig. 7 The black color gives to the experimental spectrum of KLi observed with a linearly polarized pump laser beam [12,55]. The assigned progression corresponds to transitions from the ground state levels $v" = 3$, $J" = 8$ to the levels $v' = 16$, 17, and 18, for $J' = 8$ of $2^1\Pi$. The red color gives our spectrum calculated from Eq.4 using our potential curve of $2^1\Pi$. The green color is the spectrum calculated from the program LEVEL.

only levels with widths broader then 10^{-3} cm^{-1} are presented. As expected the biggest differences between theoretical results occur for the quasi-bound states lying just below the barrier's maximum, where the semi-classical approach becomes insufficient. The differences between theoretical results and available experimental data do not exceed the experimental resolution. It means that these set of results may be useful in further assigning of experimental spectrum. The energies, widths and lifetimes of all calculated quasi-bound levels may be found in Supplementary material [28].

4 Conclusions

In order to describe the rovibrational predissociation process of the KLi molecule we calculated the low lying adiabatic potential energy curves with particular emphasis on the $2^1\Pi$ state. Our spectroscopic parameters are in a very good agreement with experimental values. A small barrier to dissociation (~ 20 cm^{-1} for $J = 0$) is identified. Having the potential curve of $2^1\Pi$ state we calculate the rovibrational levels. The differences between the successive levels are compared with those derived from experimental data. The agreement again is very good, which means that the shape of the excited electronic state $2^1\Pi$ is reliable.

Using the complementary time-dependent approach we solve the time-dependent nuclear Schrödinger equation. The solutions show the evolving wavepacket originally placed on the effective potential curve. The spectrum is calculated as a Fourier transform of the autocorrelation function. The differences between successive peaks in the spectrum are compared with the experimental spectrum. In our calculations of the time-dependent population

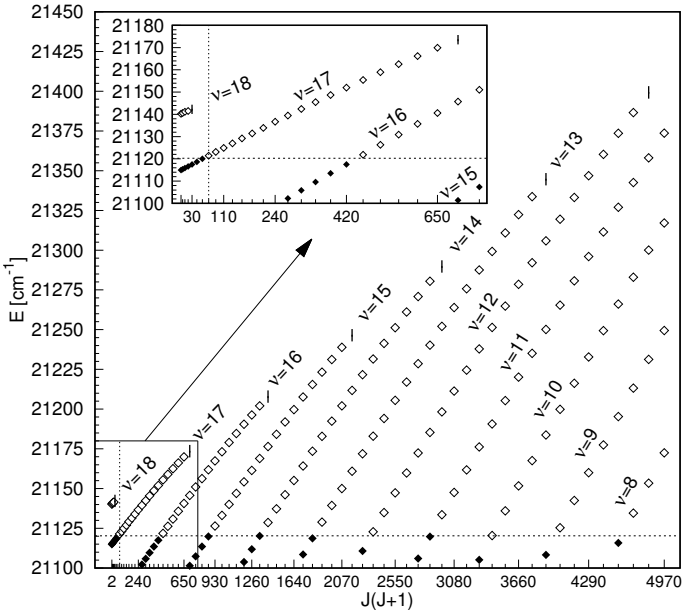

Fig. 8 Energies of term values for v = 8-18 obtained from time-dependent calculations. Full diamonds indicate bound levels, empty diamonds - quasi-bound levels, short vertical bars - the last rotational level for a chosen v.

of the rovibrational (v,J) levels, we focus on initial wavepackets chosen as eigenfunctions of quasi-bound states calculated with classical turning points. This approach allows for the exact description of the rovibrational predissociation mechanism of the KLi molecule. We show explicitly that the population of a quasi-bound state decays exponentially in time. This approach can be easily used for other diatomic and even polyatomic molecules.

We also describe the detailed procedure of calculating widths of quasi-bound vibrational levels with the high accuracy. The present method for solving TDSE is often used as a benchmark for testing other numerical methods[56]. It is especially important in the view of ultracold experiments as quasi-bond could possibly be explored for new ways of cooling molecules. states Extensive tables with calculated level energies, widths and lifetimes are presented. Those results are of considerable relevance to the design of experiments and the development of approximate computational methods. For available experimental data the comparison with our results gives very good agreement. Certainly, we hope that the results may be helpful in assigning transitions to quasi-bound levels.

Acknowledgments

This work was partially supported by the COST action XLIC (CM1204) of the European Community and the Polish Ministry of Science and Higher Education. Calculations have been carried out using resources of the Academic Computer Centre in Gdańsk.

References

1 S. A. Moses, J. P. Covey, M. T. Miecnikowski, D. S. Jin and J. Ye, *NATURE PHYSICS*, 2017, **13**, 13–20.

2 M. Wiatr, P. Jasik, T. Kilich, J. E. Sienkiewicz and H. Stoll, *Chem. Phys.*, 2018, **500**, 80–87.

3 M. Chaieb, H. Habli, L. Mejrissi, A. A. Al-Ghamdi, B. Oujia and F. X. Gadea, *INTERNATIONAL JOURNAL OF QUANTUM CHEMISTRY*, 2017, **117**, e25437.

4 J. M. Walter and S. Barrat, *Proc. R. Soc.*, 1928, **119**, 257.

5 W. Weizel and M. Kulp, *Ann. Phys.Leipzig*, 1930, **4**, 971.

6 K. ZMBOV, C. WU and H. IHLE, *JOURNAL OF CHEMICAL PHYSICS*, 1977, **67**, 4603–4607.

7 F. ENGELKE, H. HAGE and U. SPRICK, *CHEMICAL PHYSICS*, 1984, **88**, 443–453.

8 F. Sievers, N. Kretzschmar, D. R. Fernandes, D. Suchet, M. Rabinovic, S. Wu, C. V. Parker, L. Khaykovich, C. Salomon and F. Chevy, *PHYSICAL REVIEW A*, 2015, **91**, 023426.

9 E. A. Pazyuk, A. V. Zaitsevskii, A. V. Stolyarov, M. Tamanis and R. Ferber, *RUSSIAN CHEMICAL REVIEWS*, 2015, **84**, 1001–1020.

10 W. Jastrzębski, P. Kowalczyk and A. Pashov, *JOURNAL OF MOLECULAR SPECTROSCOPY*, 2001, **209**, 50–56.

11 A. Grochola, P. Kowalczyk, W. Jastrzębski, P. Crozet and A. Ross, *ACTA PHYSICA POLONICA A*, 2002, **102**, 729–738.

12 A. Grochola, W. Jastrzębski, P. Kowalczyk, P. Crozet and A. Ross, *CHEMICAL PHYSICS LETTERS*, 2003, **372**, 173–178.

13 H. Salami, A. J. Ross, P. Crozet, W. Jastrzębski, P. Kowalczyk and R. J. Le Roy, *JOURNAL OF CHEMICAL PHYSICS*, 2007, **126**, 194313.

14 A. Adohi-Krou, W. Jastrzębski, P. Kowalczyk, A. V. Stolyarov and A. J. Ross, *JOURNAL OF MOLECULAR SPECTROSCOPY*, 2008, **250**, 27–32.

15 W. Jastrzębski, P. Kowalczyk and J. Szczepkowski, *CHEMICAL PHYSICS LETTERS*, 2016, **666**, 19–21.

16 E. Wille, F. M. Spiegelhalder, G. Kerner, D. Naik, A. Trenkwalder, G. Hendl, F. Schreck, R. Grimm, T. G. Tiecke, J. T. M. Walraven, S. J. J. M. F. Kokkelmans, E. Tiesinga and P. S. Julienne, *PHYSICAL REVIEW LETTERS*, 2008, **100**, 053201.

17 A. C. Voigt, M. Taglieber, L. Costa, T. Aoki, W. Wieser, T. W. Haensch and K. Dieckmann, *PHYSICAL REVIEW LETTERS*, 2009, **102**, 020405.

18 A. Ridinger, S. Chaudhuri, T. Salez, U. Eismann, D. R. Fernandes, K. Magalhaes, D. Wilkowski, C. Salomon and F. Chevy, *EUROPEAN PHYSICAL JOURNAL D*, 2011, **65**, 223–242.

19 W. MULLER and W. MEYER, *JOURNAL OF CHEMICAL PHYSICS*, 1984, **80**, 3311–3320.

20 S. Rousseau, A. Allouche, M. Aubert-Frecon, S. Magnier, P. Kowalczyk and W. Jastrzębski, *CHEMICAL PHYSICS*, 1999, **247**, 193–199.

21 B. HURON, J. MALRIEU and P. RANCUREL, *JOURNAL OF CHEMICAL PHYSICS*, 1973, **58**, 5745–5759.

22 R. Dardouri, H. Habli, B. Oujia and F. X. Gadea, *CHEMICAL PHYSICS*, 2012, **399**, 65–79.

23 K.-L. Xiao, C.-L. Yang, M.-S. Wang, X.-G. Ma and W.-W. Liu, *JOURNAL OF QUANTITATIVE SPECTROSCOPY & RADIATIVE TRANSFER*, 2013, **129**, 8–14.

24 L. Miadowicz, P. Jasik and J. E. Sienkiewicz, *CENTRAL EUROPEAN JOURNAL OF PHYSICS*, 2013, **11**, 1115–1122.
25 O. M. Al-dossary and N. Khelifi, *RUSSIAN JOURNAL OF PHYSICAL CHEMISTRY A*, 2014, **88**, 73–84.
26 M. Musial, A. Motyl, P. Skupin and S. A. Kucharski, CONCEPTS OF MATHEMATICAL PHYSICS IN CHEMISTRY: A TRIBUTE TO FRANK E. HARRIS, PT B, 2016, pp. 201–216.
27 W. Jastrzębski, R. Kowalczyk, A. Pashov and J. Szczepkowski, *SPECTROCHIMICA ACTA PART A-MOLECULAR AND BIOMOLECULAR SPECTROSCOPY*, 2009, **73**, 117–120.
28 *Supplementary material to this article*,.
29 P. Jasik, T. Kilich, J. Kozicki and J. E. Sienkiewicz, *Chemical Physics Letters*, 2018, **695**, 119 – 124.
30 M. Wiatr, P. Jasik and J. E. Sienkiewicz, *Physica Scripta*, 2015, **90**, 054012.
31 J. Szczepkowski, P. Jasik, A. Grochola, W. Jastrzębski, J. E. Sienkiewicz and P. Kowalczyk, *The European Physical Journal Special Topics*, 2013, **222**, 2329–2333.
32 P. Łobacz, P. Jasik and J. E. Sienkiewicz, *Central European Journal of Physics*, 2013, **11**, 1107–1114.
33 P. Jasik, J. Wilczyński and J. E. Sienkiewicz, *The European Physical Journal Special Topics*, 2007, **144**, 85–91.
34 P. Jasik and J. E. Sienkiewicz, *Chemical Physics*, 2006, **323**, 563 – 573.
35 P. Fuentealba, H. Preuss, H. Stoll and L. Von Szentpály, *Chem. Phys. Lett.*, 1982, **89**, 418.
36 J. Poppe and P. Fuentealba, *Unpublished basis set*, 1988, see http://www.molpro.net.
37 I. Lim, P. Schwerdtfeger, B. Metz and H. Stoll, *J. Chem. Phys.*, 2005, **122**, 104103.
38 B. P. Prascher, D. E. Woon, K. A. Peterson, T. H. Dunning and A. K. Wilson, *Theoretical Chemistry Accounts*, 2011, **128**, 69–82.
39 H.-J. Werner, P. J. Knowles, G. Knizia, F. R. Manby, M. Schütz, P. Celani, W. Györffy, D. Kats, T. Korona, R. Lindh, A. Mitrushenkov, G. Rauhut, K. R. Shamasundar, T. B. Adler, R. D. Amos, A. Bernhardsson, A. Berning, D. L. Cooper, M. J. O. Deegan, A. J. Dobbyn, F. Eckert, E. Goll, C. Hampel, A. Hesselmann, G. Hetzer, T. Hrenar, G. Jansen, C. Köppl, Y. Liu, A. W. Lloyd, R. A. Mata, A. J. May, S. J. McNicholas, W. Meyer, M. E. Mura, A. Nicklass, D. P. O'Neill, P. Palmieri, D. Peng, K. Pflüger, R. Pitzer, M. Reiher, T. Shiozaki, H. Stoll, A. J. Stone, R. Tarroni, T. Thorsteinsson and M. Wang, *MOLPRO, version 2012.1, a package of ab initio programs*, see http://www.molpro.net.
40 R. J. Le Roy, *J. Quant. Spectrosc. Radiat. Transfer*, 2017, **186**, 167.
41 R. Schinke, *Photodissociation Dynamics*, Cambridge University Press, Cambridge, 1993.
42 M. Frigo and S. G. Johnson, *Proceedings of the IEEE*, 2005, **93**, 216–231.
43 H. Tal-Ezer and R. Kosloff, *J. Chem. Phys.*, 1984, **81**, 3967–3971.
44 R. Kosloff, *Quantum molecular dynamics on grids*, Department of Physical Chemistry and the Fritz Haber Research Center, 1997, pp. 1–75.
45 R. Kosloff, *J. Phys. Chem.*, 1988, **92**, 2087–2100.
46 J. Kozicki and F. Donzé, *Computer Methods in Applied Mechanics and Engineering*, 2008, **197**, 4429–4443.
47 J. Kozicki and F. Donzé, *Engineering Computations*, 2009, **26**, 786–805.
48 M. Abramowitz and I. Stegun, *Handbook of mathematical functions*, Dover publications, inc. New York (reprint), 2013.
49 V. Mandelshtam and H. Taylor, *J. Chem. Phys.*, 1995, **102**, 7390–7399.
50 V. Mandelshtam and H. Taylor, *J. Chem. Phys.*, 1995, **103**, 2903–2907.
51 N. E. Henriksen and F. Y. Hansen, *Theories of Molecular Reaction Dynamics: The Microscopic Foundation of Chemical Kinetics*, Oxford University Press Inc., New York, 2008.
52 A. Pashov, W. Jastrzbski and P. Kowalczyk, *Chemical Physics Letters*, 1998, **292**, 615 – 620.
53 M. Musiał and A. Bewicz, *Private communication*, 2017.
54 V. Bednarska, I. Jackowska, W. Jastrzębski and P. Kowalczyk, *Journal of Molecular Spectroscopy*, 1998, **189**, 244–248.
55 A. Grochola, *Investigation of the electronic structure of alkali metal dimers using the polarization spectroscopy technique*, 2004, PhD Thesis.
56 C. Leforestier, R. Bisseling, C. Cerjan, M. Feit, R. Friesner, A. Guldberg, A. Hammerich, G. Jolicard, W. Karrlein, H. Meyer, N. Lipkin, O. Roncero and R. Kosloff, *Journal of Computational Physics*, 1991, **94**, 59–80.

Table 3 Energies and widths of chosen quasi-bound levels from the $2^1\Pi$ state. Present results obtained by time-dependent calculations (Present,TDSE) and by means of the program LEVEL (Present) are compared with those measured in the experiment[27]. Only levels with the f rotational symmetry are listed. The double column ΔE gives differences between Experiment and respectively Present,TDSE and Present. $\Delta\Gamma$ gives the relative difference between level widths calculated as (Present - Present,TDSE)/Present,TDSE.

		Energy $[cm^{-1}]$				Width Γ $[cm^{-1}]$		
J	v	Present,TDSE	Present	Experiment[27]	ΔE	Present,TDSE	Present	$\Delta\Gamma$
1	18	21140.338	21140.449			1.2580	1.3698	0.089
2	18	21140.605	21140.720			1.3096	1.4321	0.094
3	18	21141.006	21141.122			1.3787	1.5282	0.108
4	18	21141.507	21141.643			1.4948	1.6508	0.104
5	18	21142.175	21142.238			1.6331	1.7715	0.085
17	17	21142.408	21142.423	21142.417	0.009, -0.006	2.4877×10^{-3}	2.4938×10^{-3}	0.002
18	17	21145.514	21145.509	21145.434	-0.080, -0.075	7.3878×10^{-3}	7.4499×10^{-3}	0.008
19	17	21148.720	21148.719	21148.553	-0.167, -0.166	2.0125×10^{-2}	2.0341×10^{-2}	0.011
20	17	21152.026	21152.037	21151.714	-0.312, -0.323	4.9872×10^{-2}	5.0865×10^{-2}	0.020
21	17	21155.433	21155.451	21155.066	-0.367, -0.385	1.1437×10^{-1}	1.1653×10^{-1}	0.019
22	17	21158.939	21158.948	21158.400	-0.539, -0.548	2.4177×10^{-1}	2.4461×10^{-1}	0.012
23	17	21162.513	21162.521	21161.830	-0.683, -0.691	4.7034×10^{-1}	4.7253×10^{-1}	0.005
24	17	21166.153	21166.174			8.3086×10^{-1}	8.4896×10^{-1}	0.022
25	17	21169.860	21169.917			1.3596	1.4341	0.055
26	17	21173.594	21173.538			2.0983	2.1353	0.018
30	16	21167.455	21167.465	21167.380	-0.075, -0.085	1.5023×10^{-3}	1.5443×10^{-3}	0.028
31	16	21173.133	21173.152	21172.888	-0.245, -0.264	6.7315×10^{-3}	6.8733×10^{-3}	0.021
32	16	21178.877	21178.906	21178.406	-0.471, -0.500	2.5554×10^{-2}	2.5844×10^{-2}	0.011
33	16	21184.688	21184.702	21183.965	-0.723, -0.737	8.1813×10^{-2}	8.2820×10^{-2}	0.012
34	16	21190.499	21190.509	21189.630	-0.869, -0.879	2.2249×10^{-1}	2.2701×10^{-1}	0.020
35	16	21196.309	21196.311			5.2662×10^{-1}	5.3651×10^{-1}	0.019
36	16	21202.087	21202.120			1.0863	1.1147	0.026
37	16	21207.864	21207.938			1.9701	2.0734	0.052
40	15	21199.716	21199.713	21199.333	-0.383, -0.380	1.7736×10^{-3}	1.7881×10^{-3}	0.008
41	15	21207.564	21207.593	21206.890	-0.674, -0.703	8.7548×10^{-3}	8.9113×10^{-3}	0.018
42	15	21215.479	21215.488			3.6380×10^{-2}	3.6912×10^{-2}	0.015
43	15	21223.327	21223.358			1.2539×10^{-1}	1.2745×10^{-1}	0.016
44	15	21231.141	21231.163			3.6025×10^{-1}	3.6692×10^{-1}	0.019
45	15	21238.856	21238.891			8.7055×10^{-1}	8.8924×10^{-1}	0.021
46	15	21246.504	21246.573			1.7858	1.8662	0.045
49	14	21241.327	21241.345			4.2147×10^{-3}	4.2525×10^{-3}	0.009
50	14	21251.246	21251.231			2.0288×10^{-2}	2.0543×10^{-2}	0.013
51	14	21261.064	21261.066			8.1186×10^{-2}	8.2309×10^{-2}	0.014
52	14	21270.782	21270.793			2.6828×10^{-1}	2.7182×10^{-1}	0.013
53	14	21280.367	21280.376			7.3356×10^{-1}	7.4032×10^{-1}	0.009
54	14	21289.785	21289.840			1.6714	1.6977	0.016
56	13	21275.625	21275.668			1.2668×10^{-3}	1.2967×10^{-3}	0.024
57	13	21287.447	21287.484			7.1898×10^{-3}	7.3604×10^{-3}	0.024
58	13	21299.236	21299.248			3.3983×10^{-2}	3.4759×10^{-2}	0.023
59	13	21310.891	21310.900	21309.310	-1.581, -1.590	1.3478×10^{-1}	1.3582×10^{-1}	0.008
60	13	21322.379	21322.373			4.3449×10^{-1}	4.3478×10^{-1}	0.001
61	13	21333.634	21333.644			1.1463	1.1435	-0.002
62	13	21344.721	21344.746			2.5271	2.5240	-0.001